# MESO SCALE ANALYSIS OF DAMAGE AND STIFFNESS DEGRADATION IN NON-CRIMP FABRIC COMPOSITES

Dmitry S. Ivanov[1], Stepan V. Lomov[1], Thanh Troung Chi[2], Dmitry Klimshin[3], Ignaas Verpoest[1]

E-mail: dmitry.ivanov@mtm.kuleuven.be, Tel.: +32-16-321-317

[1]Katholieke Universiteit Leuven Kasteelpark Arenberg, 44 B-3001 Leuven (Heverlee) Belgium

[2]Can Tho University, 10000, 3/2 street , Can Tho, Vietnam

[2]St.Petersburg State Technical University, 195251, Polytechnicheskaya 29, St.Petersburg, Russia

## ABSTRACT

Meso-scale (level of fibre bundle) analysis of damage in non-crimp fabric (NCF) composites of sheared configurations is presented. Modelling is performed by means of continuous damage mechanics and local analysis of failure within a unit cell. The finite element (FE) model of the composite unit cell accounts for the geometry of resin rich zones caused by the stitching distortions. The damage evolution law of Ladeveze is employed in conjunction with the degradation scheme of Murakami and Puck criterion. Experiments serve twofold: (1) to adjust parameters for damage modelling (tensile tests of ± 45° lay-up at different fibre volume fractions), (2) to verify the modelling. The model describes non-linearity of the stress-strain diagrams during the tensile tests, strain at initiation of matrix intra-ply cracking and final failure.

## 1 INTRODUCTION

Biaxial non-crimp stitched carbon fabric (NCF) reinforced epoxy composites are explored. The textiles are pre-sheared before the impregnation to study influence of the draping on mechanical properties. The study is performed both experimentally and numerically focusing on the meso-scale, where individual fibre bundles and matrix resin rich zone caused by stitching distortions are distinguished. The purpose of the research is to predict stiffness degradation, damage initiation and final failure based on meso-scale geometry and properties of unidirectional (UD) composites. The latter are extracted from tensile tests of UD and ±45° non-crimp composites.

The NCF composites were extensively investigated in recent years. Greve [1] approximated the internal structure of sheared NCF composites by UD laminates and adopted damage mechanics of Ladeveze [2] to describe the stiffness degradation. The final failure was predicted by Puck criterion [3]. Edgren [4] accounted for waviness and resin rich zones in 2D model of NCF composite. The degradation was described by micro mechanical models developed for analysis of conventional laminated composites.

Here, 3D FE models of sheared NCF composites are presented. The models account for the geometry of the distortions induced by stitching and local fibre volume distribution around them. The accent is done on local meso stress distribution within the UD fibre bundles. Following [1], damage evolution law of Ladeveze is employed to govern the shear modulus reduction. The degradation of the transverse properties is introduced via Murakami degradation scheme [5], which is based on clear geometrical meaning of the damage parameter. The transverse degradation “switches”, when the Puck criterion [3] (implemented locally) indicates the transverse intra-ply crack occurrence. Hence, the

presented modeling focuses on the structural features, which govern meso stress distribution and damage accumulation process.

Meso model is verified against macro parameters (elastic moduli and tensile diagrams) and meso features (the damage onset). Experimentally, the damage initiation is registered by acoustic emission measurements and posterior X-Ray examination [6, 7]. Tensile tests of ±45° non-crimp composites serve to extract parameters of the damage evolution law.

## 2 GEOMETRY AND TEST DESCRIPTION

### *2.1 Material and specimens*

The bi-axial multi-ply carbon reinforcement fabrics (Figure 1a) are stitched by Polyester (PES) yarns in Tricot pattern with a weight of 7.6 tex and an areal density of 6 g/m² (2 % of total weight). The stitching has no other function but to bind the plies together. Pattern of polyester yarns induces long distortions triangular in plane [8]. Dispersed glass yarns in between 0° and 90° plies serve to stabilise the material. The textiles are produced based on the UD plies with an areal density of approximately 150 g/m².

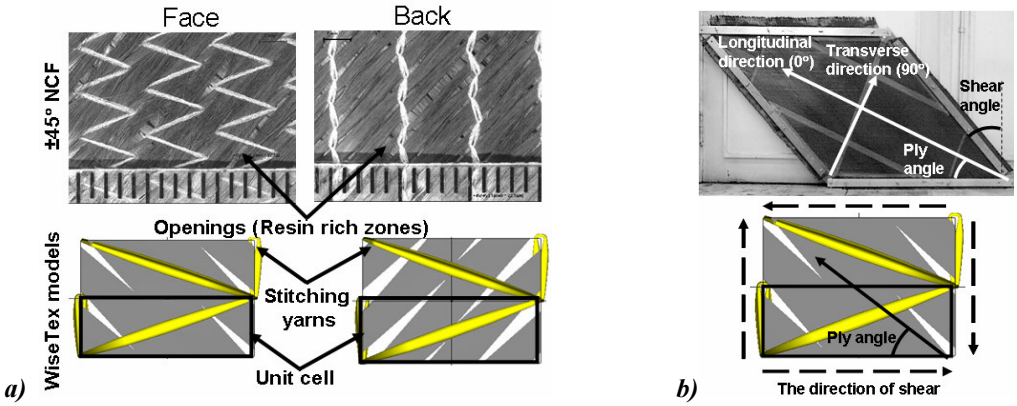


**Figure 1** *a) In plane geometry of the fabric and geometrical model of unit cells (produced in WiseTex [8]); b) shearing of the textile: shear frame and the unit cell deformation;*

The biaxial fabrics were sheared at 30º, 45º and 50º (corresponds to the ply angles ± 30º, ± 20º, ± 22.5º – Figure 1b) in an aluminium frame. After every 5º of the shear, the fabric was left in the frame for some time to allow for its relaxation [6]. The maximum shear angle (50º) is close to the shear locking angle of the fabric. The geometrical features of the textile were measured on the dry fabric [9] – Table 1.

**Table 1. Geometrical properties of the biaxial NCF composites**

| ***Shear angle, °*** | *0* | *0* | *30* | *50* |
|---|---|---|---|---|
| ***Fibre orientation, °*** | ± 45 | ± 45 | ± 30 | ± 20 |
| ***Total fibre volume fraction, %*** | 22.6 | 39.4 | 24.2 | 39.4 |
| ***Volume fraction of openings, %*** | 12.0 | 12.0 | 7.4 | 10.0 |
| ***Number of plies*** | 16 | 8 | 8 | 8 |
| ***Thickness of the composite, mm*** | 3.5 | 3.0 | 3.0 | 3.0 |
| ***Unit cell dimensions, mm× mm*** | 4.9 × 1.7 | 4.9 × 1.7 | 3.46 × 2.08 | 2.37 × 2.26 |
| ***Distortion width: face/back, mm*** | 0.28 ± 0.01/ 0.43 ± 0.02 | 0.28 ± 0.01/ 0.43 ± 0.02 | 0.18 ± 0.01/ 0.44 ± 0.02 | 0.21 ± 0.02/ 0.33 ± 0.02 |
| ***Distortion length: face/back, mm*** | 5.05 ± 0.29/ 7.15 ± 0.27 | 5.05 ± 0.29/ 7.15 ± 0.27 | 4.75 ±0.20/ 5.40 ± 0.28 | 4.66 ± 0.22/ 4.97 ± 0.32 |

The non-sheared composites are presented by two configurations of high and low fibre volume fractions (22.6 and 39.4 %), which was achieved by varying number of the plies. Hence, the damage parameters can be extracted for a range of fibre volume fractions. The composites were manufactured by Resin Transfer Moulding [6].

## 2.2 *Tensile test*

Quasi-static tensile tests were displacement controlled and performed with a speed of 3 mm/min. To register the displacement during the test, extensometers with a gauge length of 50 mm and 25 mm respectively were attached to the specimens (dimensions 25×250 mm). The acoustic emission sensors were placed on the same side of the specimen with a distance of 110 mm between them. Signals from the sensors were afterwards analysed and those signals coming from the grips were filtered out. Tests were performed in the non-fibre directions of the orthotropy – 0º and 90º. The tensile diagrams of the tests in longitudinal 0º direction are presented on Figure 2.

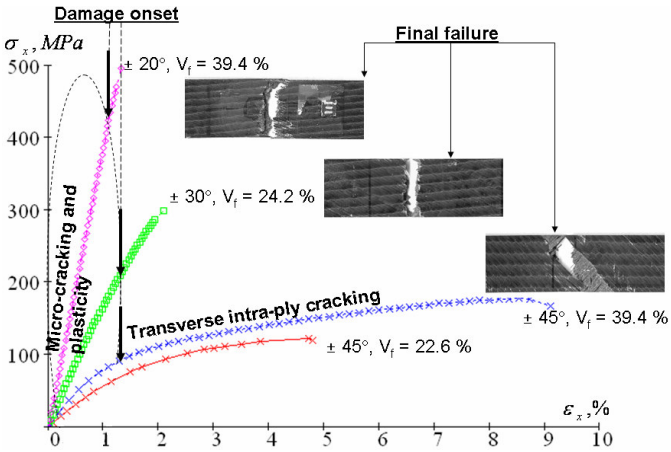


**Figure 2**. *Tensile tests of NCF composites in longitudinal direction (Vf – fibre volume fraction, ± 20º, ± 30º, ± 45º – the ply angles).*

The ± 45º specimens exhibit highly non-linear behaviour with the large deformation at failure. The non-linearity and the strain at failure decrease with the shear angle growth. The mechanism of the failure is also different. In the non-sheared configurations extensive transverse cracking is accompanied by delaminations, which further leads to the fibre pull-out and separation of the specimen. Failure of the sheared composites is due to the fibre rupture.

## 2.3 *Damage initiation registration*

The strain at the crack initiation was determined by the acoustic emission measurements. Then, samples loaded to this strain were X-Rayed to verify the crack occurrence. The pre-loaded samples were immersed in the solution of a penetrant, so that the cracks could be seen with sufficient contrast. The X-Ray images were compared with those obtained on unloaded samples. Apart from the cracks, stabilising glass yarns and resin rich zones indicating fibre direction can be seen. For all the discussed samples the damage initiation strain values are close – 1.0-1.3 %.

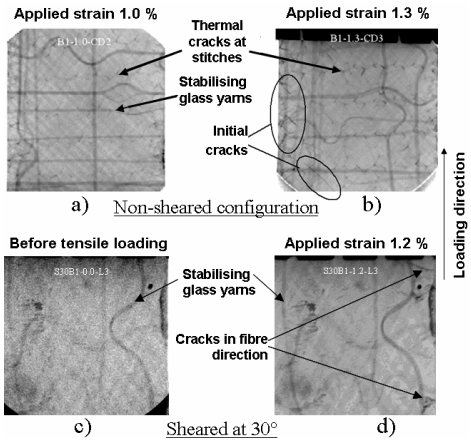


**Figure 3**. *X-Ray images of the non-sheared (a, b) and sheared specimen (c,d) before and after the damage initiation.*

The X-ray images of the non-sheared specimens loaded at 1.0 % (Figure 3a) show mainly short local thermal cracks (the same could be seen on the unloaded specimens), which develop along the stitching yarns. At 1.3 % of applied strain long transverse intra-ply cracks occur. At the initial stage there are very few cracks over the specimen (Figure 3b).

The X-ray images of the sheared (30°) specimens before and after applying tensile loads are depicted in Figure 3(c,d). In the images of the specimens before loading (Figure 3c) only the stabilising yarns can be seen and no thermal cracks are observed. On the other hand, after applying tensile loads – some short matrix cracks in the fibre directions are

found. Unlike the non-sheared materials, the cracks develop mainly from edges of the specimens. Summary of the failure and stiffness characteristics is presented in Table 2.

**Table 2 Stiffness and damage features of the biaxial composites:** Experiment / ***FEA***

| Shear angle (Ply angle),° | Fibre volume fraction (%) | Young modulus, GPa | Poisson's ratio | Strain at matrix crack onset , % | Strain at failure, (%) | Stress at failure, MPa |
|---|---|---|---|---|---|---|
| 0 (±45) | 22.6 | 9.9±0.4 / ***9.85*** | 0.83±0.04 / ***0.83*** | 1.30 / ***1.23*** | 8.7±0.3 n/a | 177.4±3.9 n/a |
| 0 (±45) | 39.4 | 6.6±0.3 / ***6.27*** | 0.69±0.02 / ***0.80*** | n/a ***2.89*** | 4.5±0.5 n/a | 121.7±5.1 n/a |
| 30 (±30) | 24.2 | 18±1.6 / ***21.1*** | 1.21±0.08 / ***1.46*** | 1.30 ***2.67*** | 2.1±0.2 / ***2.02*** | 298.7±20.9 / ***329.3*** |
| 50 (±20) | 39.4 | 44.4±4.8 / ***52.44*** | 1.18±0.11 / ***1.44*** | 1.0 ***1.72*** | 1.3±0.2 ***1.0*** | 495.6±37.4 ***399.54*** |

## *2.4 Data processing*

The tensile tests of the UD ±45° laminates serve to define the damage parameters [1] and in-plane shear response. The stress-strain state in the plies corresponds to almost pure shear conditions. According to ASTM Standard D 3518 [10] the ply shear stress $\tau_{12}$ and strain $\gamma_{12}$ in UD plies can be estimated as following:

$$\tau_{12} = \frac{\sigma_y}{2} \qquad \gamma_{12} = \varepsilon_y - \varepsilon_x \tag{1}$$

where x, y – is the global coordinate system (y – is the direction of loading), 1,2 – is the local one (1 – is the fibre direction), $\sigma_y, \varepsilon_y$ – is the stress-strain response in tensile test, $\varepsilon_x = -\nu_{yx}\varepsilon_y$ – is the lateral strain, $\nu_{yx}$ – is the Poisson's ratio.

The resin rich zones in the plies of the NCF composites occupy up to 12 %. Therefore, in order to get the shear diagrams for UD composite, a certain assumptions have to be done. The iso-strain state (used in classical laminate plate theory) can be suggested as a rough estimation. Then, the stress within the ply can be found with respect to the volume fraction of the resin rich zone $V_m$ and shear modulus of the epoxy matrix $G_m$:

$$\tau_{12} = \left( \frac{\sigma_y}{2} - V_m G_m \varepsilon_y (1+\nu_{yx}) \right) \frac{1}{1-V_m} \tag{2}$$

The resulting diagrams are given in Figure 4a.

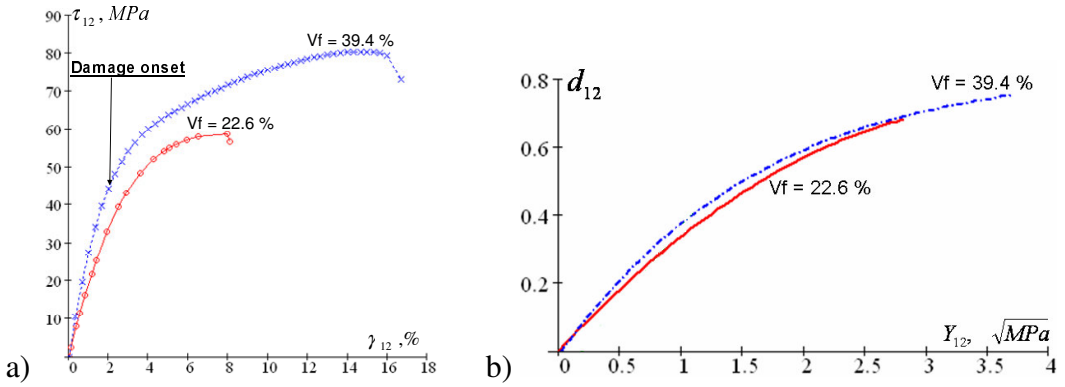


**Figure 4**. *a) The shear diagrams for two fibre volume fractions (Vf), b) Degradation of secant shear modulus with the respect to the damage fictitious force;*

The dependence of the shear diagram on the fibre volume fraction is explicit. The highest non-linearity follows the damage initiation threshold. The drop of the secant modulus at the damage initiation is about 35 %, whereas at the failure it is about 86 %. There are two factors, explaining the "switch" in the mechanical response: (1) degradation due to the transverse cracking, (2) fiber scissoring: in [10] it is suggested that fiber rotation of 1º takes place for every 2% of axial strain.

The pre-cracking non-linearity comes from the plastic deformations and micro-damage (e.g. fibre-matrix debonding and dispersed fibre splitting). For describing the degradation due to the micro-damage, the shear diagrams can be presented in a form of damage evolution law. The latter operates with the parameter responsible for the stiffness degradation $d_{12}$ and damage fictitious force $Y_{12}$, defined as partial derivative of the elastic work of the damaged material $\Psi$ with respect to the damage parameter:

$$G_{12} = G_{12}^0(1-d_{12}) \qquad Y_{12} = \sqrt{\underset{\tau \le t}{Sup}\left(\frac{\partial}{\partial d_{12}}\Psi\right)} = \underset{\tau \le t}{Sup}\left(\frac{\langle \tau_{12} \rangle}{\sqrt{2G_{12}^0}}\frac{1}{(1-d_{12})}\right) \tag{3}$$

where $G_{12}^0$, $G_{12}$ – are the shear moduli of the intact and damaged plies. The evolution law $d_{12}(Y_{12})$ is analogical to the crack-growth resistance curve in classical fracture mechanics, where the damage parameter plays a role of the crack length, and $Y_{12}$ is associated with the energy release rate. Ladeveze [2] used linear relation between $d_{12}$ and $Y_{12}$, Greve [1] proposed an exponential form. In the current work the material function $d_{12}(Y_{12})$ is reconstructed from the shear diagram. Hence, it assumed that secant modulus of the diagram at any point is close to the stiffness of the damaged ply. Therefore the plastic deformations are neglected and micro-damage is assumed to play the dominant role at the initial stage of the deformation. Since no unloading is modeled, the assumption does not introduce a significant error.

The resultant damage evolution laws are presented on Figure 4b. The remarkable particularity of these diagrams is that they are almost identical for two different fibre volume fractions. Hence, the same dependence will be used for modelling of all the studied NCF composites. The following cubic polynom approximates the experiments:

$$d_{12} = -0.0053 + 0.4848Y_{12} - 0.1122Y_{12}^{\ 2} + 0.0099Y_{12}^{\ 3} \tag{4}$$

## 3 FE MODELLING

### *3.1 FE models*

The meso-approach requires building the geometrical model of representative volume element of the composite. In the proposed model the crimp/waviness of the plies is neglected. The stitching yarns are excluded for simplicity: their stiffness contribution is close to the one of the matrix. The effect stitching is accounted by introducing matrix resin rich zones of proper dimensions. The distortions cause local variation of orientation and volume fraction of the fibres. The latter was introduced as a linear function of the distance from the distortion boundaries. The "disturbed" area width is of the same size as the local distortion width. Local elastic properties of the fibrous bundles are calculated based on analytical formulas of Chamis [11], where fibre volume fraction and the elastic properties of the fibres and matrix are the input parameters.

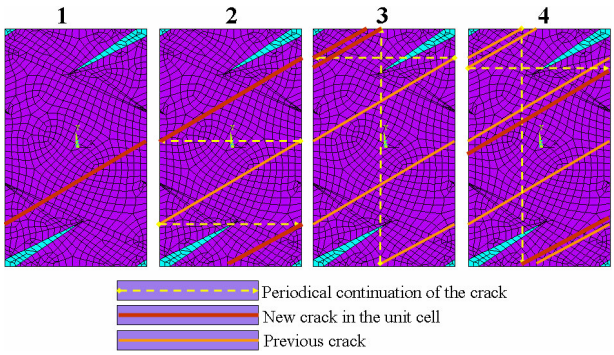


**Figure 5.** *Illustration of the non-periodical nature of the damaged composite;*

There should be a hypothesis describing an interaction of the representative volume element with its neighbours. The unit cell of the reinforcement is traditionally chosen as the basic geometrical entity. It is embedded in the self-similar structure and the periodicity assumption can be made about the meso stress and strain. This assumption leads to the periodic boundary conditions restraining displacement on the opposite side of the unit cell [12]. The meshed unit cells of individual plies and the entire layer are shown on Figure 5. The results of the elastic homogenisation are given in Table 2.

The matrix intra-ply crack occurrence breaks the periodicity assumption. The cracks in NCF composite often cross the entire width of specimen. Figure 5 shows the consequent modelling of the crack propagation: on the first stage the crack is unique: it runs through out the unit cell ending at left and right boundaries. Periodicity leads to occurrence of the two new continuations of the crack, which also cross the cell leading to two new "endings". The process continues until the cell turns to dust. Hence, this geometrical peculiarity governs the choice of an instrument for the damage modelling. Continuous damage mechanics can describe the degradation of the entire fibrous region without diving into the local geometry of a crack or a damage zone.

### *3.2 Modelling of the non-linearity*

In the current work it is assumed that all the fibrous plies degrade entirely responding to average stress-strain state in it. The rule of the degradation is chosen based on the damage mechanics of Ladeveze [2]. According to this approach there are two damage parameters responsible for the stiffness reduction under the transverse cracking: $d_2$ (for the transverse Young's modulus) and $d_{12}$ (for the shear modulus). In [2] coupling between these two parameters is introduced in a damage evolution law.

Alternatively, these parameters can be related by the degradation scheme (called here the Murakami scheme [5]), which is based on the principle of strain equivalence imposed by the continuous damage mechanics [13]. The latter has explicit geometrical meaning: it introduces the damage parameter as area fraction of the degraded zone projection on the coordinate planes. Then, based on energy notion, the degraded stiffness matrix is written as (the plane case is shown for simplicity, cracks in the plane 1-3 are assumed):

$$C^d = \begin{pmatrix} C_{11}^0 & C_{12}^0(1-d_2) & 0 \\ & C_{22}^0(1-d_2)^2 & 0 \\ sym. & & G_{12}^0\left(\frac{2(1-d_2)}{2-d_2}\right)^2 \end{pmatrix} \tag{5}$$

where $C_{ij}^0$ are the stiffness of the intact material. Comparison with definition of $d_{12}$ (3) gives the link between the two parameters:

$$d_2 = \frac{2(1-\sqrt{1-d_{12}})}{(2-\sqrt{1-d_{12}})} \tag{6}$$

The single damage parameter approach is more convenient and easy to implement and hence will be used further in connection to the damage evolution law. The degradation of the transverse modulus $d_2$ is much less pronounced than the degradation of the shear modulus $d_{12}$. Greve [1] used a simplified scheme, where only $d_{12}$ was accounted for. Therefore, the shear degradation is chosen as a governing parameter, while $d_2$ can be expressed in terms of $d_{12}$.

The transverse degradation is only accounted for the transverse cracking (i.e. after the damage onset). The degradation of the composite is determined by the crack opening displacement [4]. It is assumed that the micro cracking influences the shear response only, since the planes of micro-cracks are not well-defined as in the case of meso intra-ply cracks. Hence, the equation (6) is modified as:

$$d_2 = \begin{cases} 0 \quad if \quad d_{12} < d_{12}^X \\ \dfrac{2(1-\sqrt{1-(d_{12}-d_{12}^X)})}{(2-\sqrt{1-(d_{12}-d_{12}^X)})} \quad if \quad d_{12} \geq d_{12}^X \end{cases} \tag{7}$$

where $d_{12}^X$ – is damage parameter corresponding to the load level when the transverse cracking occurs.

The presented approach can be described as a step-wise procedure: first a boundary value problem is solved and the average shear stress in the pure UD regions is calculated. The meso-damage initiation criterion (see the next paragraph) is employed to check if $d_{12} = d_{12}^X$. The shear degradation and related transverse degradation parameters are estimated based on the equations (4) and (7). Then, the degradation is assigned to the UD bundles of the plies and the boundary value problem is solved again (at the same load step) to calculate the effective response of the damaged composite.

### *3.3 Modelling of damage initiation*

The initial damage with transverse cracking is analysed with the Puck criterion [3] benchmarked by the World-Wide Failure Exercise [14]. Unlike the modelling of degradation (where the average stress governs degradation of UD plies), the criterion is applied locally to account for the stress distribution induced by the distortions. The criterion introduces the stress exposure factor (SEF), which characterises risk of failure on so-called "action plane" (defined around the fibre axis by the angle θ):

$$SEF(\theta) = \begin{cases} \sqrt{\left(\dfrac{p_{\perp\psi}^{(-)}}{R_{\perp\psi}^A}\right)^2 \sigma_n{}^2 + \left(\dfrac{\tau_{nt}}{R_{\perp\perp}^A}\right)^2 + \left(\dfrac{\tau_{n1}}{R_{\perp\parallel}}\right)^2} + \dfrac{p_{\perp\psi}^{(-)}}{R_{\perp\psi}^A}\sigma_n \quad for \quad \sigma_n \geq 0 \\ \sqrt{\left(\dfrac{1}{R_{\perp}^{(+)}} - \dfrac{p_{\perp\psi}^{(+)}}{R_{\perp\psi}^A}\right)^2 \sigma_n{}^2 + \left(\dfrac{\tau_{nt}}{R_{\perp\perp}^A}\right)^2 + \left(\dfrac{\tau_{n1}}{R_{\perp\parallel}}\right)^2} + \dfrac{p_{\perp\psi}^{(+)}}{R_{\perp\psi}^{(+)}}\sigma_n \quad for \quad \sigma_n < 0 \end{cases} \tag{8}$$

where σ,τ are the normal and shear stress acting on the action plane (n – is the index of coordinate normal to the plane, 1 – is the fibre direction and t- is the in-plane coordinate, the indexes ∥ and ⊥ - define the fibre and transversal direction of the UD yarn segment). The crack is assumed to appear when SEF=1 at any possible angle θ. The input parameters (such as basic strengths $R_{\perp\parallel}, R_{\perp}$, critical stressing values $R^A$, and inclination parameters $p$) are given in Table 3. These parameters were measured for different fibre volume fractions

of the UD composite than those used in the model. However, as it was shown by Skudra [15], the transverse and shear strength of the UD composite almost do not depend on the fibre volume fraction due to the low contrast of transverse stiffness of the carbon fibres and stiffness of the matrix (the stress concentration on the micro level plays a decisive role for the strength values). It was assumed that the other parameters used in the study (such as the inclination parameter in Puck criterion) are also not sensitive to it.

**Table 3**. *Strength and inclination parameters of Puck criterion;*

| **Parameters based on measurements** | | | | |
|---|---|---|---|---|
| $R_{\perp}^{(+)}$, MPa | $R_{\perp}^{(-)}$, MPa | $R_{\perp\parallel}$, MPa | $p_{\perp\parallel}^{(+)}$ | $p_{\perp\parallel}^{(-)}$ |
| 28* | 230* | 74* | 0.35** | 0.3** |
| **Estimated parameters** | | | | |
| $R_{\perp}^{A} = R_{\perp}^{(+)}$, MPa | $R_{\perp\parallel}^{A} = R_{\perp\parallel}$, MPa | $R_{\perp\perp}^{A} = R_{\perp\perp}^{(-)} \frac{1}{2\left(1 + p_{\perp\perp}^{(-)}\right)}$, MPa | $p_{\perp\perp}^{(-)} = \frac{1}{2}\left(\sqrt{1 + 2p_{\perp\parallel}^{(-)} \frac{R_{\perp}^{(-)}}{R_{\perp\parallel}}} - 1\right)$ | |
| 28 | 74 | 85.4 | 0.346 | |

***-[6], **-[3]**

The fibre failure is governed by the normal stress along the fibres $\sigma_1$. Critical stress level $\sigma_1^{cr}$ at the arbitrary volume fraction $V_f$ is often predicted fairly well by the simple rule of mixture:

$$\sigma_1^{cr}(V_f) = \sigma_{mtr}^{cr} + (\sigma_1^{cr}(\overline{V}_f) - \sigma_{mtr}^{cr})\frac{V_f}{\overline{V}_f} \tag{9}$$

where $\sigma_1^{cr}(\overline{V}_f)$ – is the strength of UD composite with fibre volume fraction $\overline{V}_f$, $\sigma_{mtr}^{cr}$ – is the tensile strength of the matrix. For this carbon-epoxy system the measured UD strength is $\sigma_1^{cr}(42.9\%) = 1317.3MPa$, $\sigma_{mtr}^{cr} = 70.1MPa$. Unlike the matrix inter-ply crack, the fibre crack crosses the entire specimen at once leading to the catastrophic failure. Therefore local meso stress $\sigma_1$ was checked to predict the fibre dominated rupture of the specimen.

## 4 RESULTS AND DISCUSSION

The matrix intra-ply crack initiation is predicted well for the non-sheared configuration (6 % error –Table 2, Figure 6) via the Puck criterion.

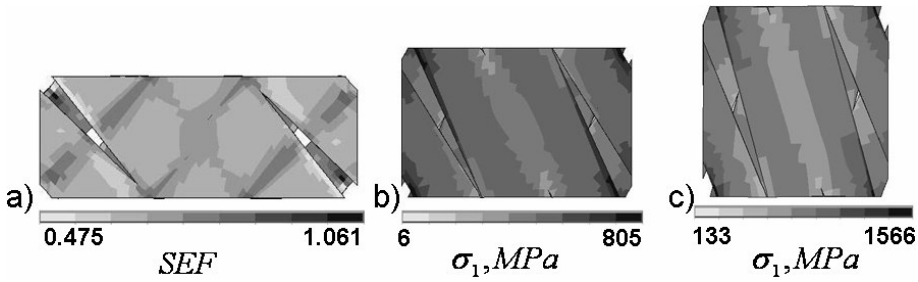


**Figure 6.** *(a) Stress exposure factor (SEF) for ± 45° composite at applied deformation 2,1 % , (b) Longitudinal (fibre) stress for ± 30° at 2,1 %, (c) Longitudinal stress for 50 at 1.3 %.*

For the pre-sheared composites the intra-ply cracking is estimated beyond the final failure registered in the experiments and predicted by the fibre rupture criterion (9). It should be noticed though, that all the matrix cracks in the sheared composites initiated at the specimen edges. Periodic boundary conditions do not account for the loading conditions at the edge, where according to common observations (for heterogeneous materials) the stress

concentration is higher. The critical strain at the fibre rupture is predicted close to the experimental values. Hence, the mode of macro failure is modelled properly.

Secant moduli reduction is given in Figure 7. The analysis describes the non-linearity well in accordance with the experimental data. It shows that the assumptions used for obtaining of the shear diagrams were generally correct. The numerical tests for ±45° composites tests were stopped at 3 % of applied deformation since the input data did not account for the "scissoring effect" and the experimentally obtained damage evolution law beyond this deformation stage does not make much sense.

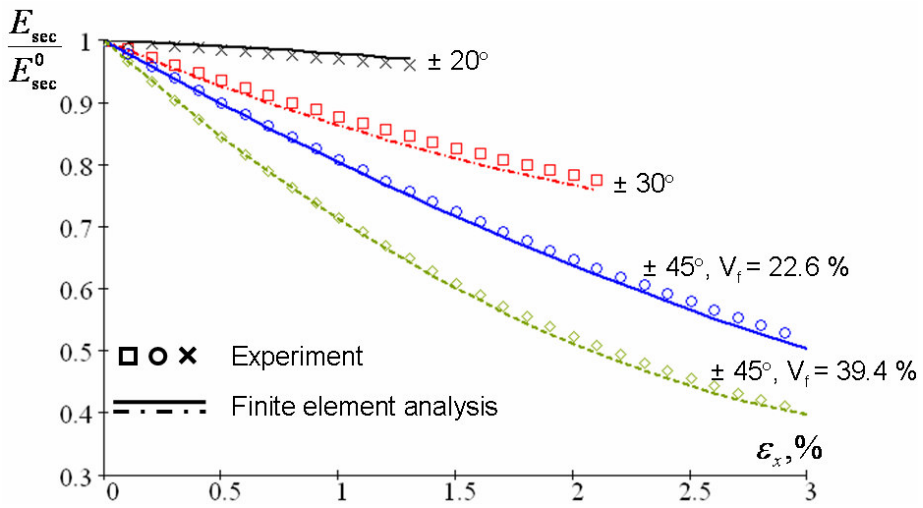


**Figure 7**. *Normalised secant moduli* $E_{sec}$ *in the tensile tests of NCF composites.*

It is remarkable that all the NCF composites were described by the same damage evolution law, which shows to be independent on the fibre volume fraction variation and the local ply orientation. During the degradation of the sheared composite the transverse degradation was not "switched on" due to the earlier fibre failure. The transverse degradation was present in tests of the non-sheared composites; however it did not influence the overall stiffness response (determined mainly by the shear modulus). The latter proves that ±45° tests can be used as the source data for obtaining the shear diagram of the UD composite.

## 5 CONCLUSIONS

The meso-scale approach shows good potential in predicting of the stiffness degradation, the damage onset and the final failure. The assumptions used here include absence of "scissoring", plasticity in the resin rich zones, the stitching and stabilising yarns presence, and the ply waviness. Nevertheless, the mechanical behaviour of different composites is described generally correct. The presented approach is limited by the active loading, since no plastic deformation is considered. However, it can be generalised provided the required input (loading-unloading tensile tests).

The meso scale analysis gives an important overview on the matrix intra-ply crack initiation. This requires local stress analysis and accounting for the stress concentration caused by the local geometrical features. The modelling was unable to predict the edge crack occurrence, which is out of the scope of this study due to the assumption of the unit cell periodicity. However, the edge effects did not influence much the mechanical response.

The prediction of the local crack initiation allows switching the degradation of transverse stiffness on. The latter is related to the "governing" shear degradation by the scheme of Murakami. The validation of the combined degradation scheme is still to be performed,

since the fibre failure in the sheared composites occurred earlier than the matrix crack onset. At this stage, the shear degradation of the ply is shown to be the dominant mechanism responsible for the non-linearity of the carbon-epoxy composites.

## ACKNOWLEDGEMENTS

The work has been done in the framework of EU funded ITOOL project, KULeuven grant for East-European students. The bi-axial multi-ply carbon reinforcement fabrics were provided by Saertex Wagener GmbH & Co as part of the TECABS projects (Technologies For Carbon Fibre Reinforced Modular Automotive Body Structures). Authors express gratitude to Dr. Sergey Ivanov for important discussions.

## REFERENCES

1 **Greve L., Pickett A.K.** Modelling damage and failure in carbon/epoxy non-crimp fabric composites including effects of fabric pre-shear, *Composites: Part A,* 37 (2006): 1983–2001.

2 **Ladeveze P., Lubineau G.** An enhanced mesomodel for laminates based on micromechanics *Compos Sci Technol* 62 (2002): 533–541

3 **Puck A., Kopp J., Knops M.** Guidelines for determination of the parameters in Puck's action plane strength criterion, *Compos Sci Technol*, 62(2002): 371-378.

4 **Edgren F., Mattsson D., Asp L.E., Varna J.** "Formation of damage and its effects on non-crimp fabric reinforced composites loaded in tension", *Composite Science and Technology* **64** (2004), 675-692

5 **Murakami, S.** Mechanical modeling of material damage*. J Applied Mech*, 1988; **55**: 280

6 **Truong Chi T., Vettori M., Lomov S. V., Verpoest, I.** Carbon composites based on multiaxial multiply stitched preforms. Part 4: Mechanical properties of composites and damage observation, *Composites: Part A*, 36 (2005): 1207-1221.

7 **Lomov S.V., Ivanov D.S., Truong T.C., Verpoest I, Baudry F., Vandenbosche K., Xie H.** Experimental methodology of study of damage initiation and development in textile composites in tensile test, *Compos Sci Technol* (Accepted, in press).

8 **Verpoest, I. Lomov S.V.** Virtual textile composites software Wisetex: integration with micro-mechanical, permeability and structural analysis, *Compos Sci Technol*, 2005; **65**(15-16): 2563-2574.

9 **Loendersloot R.,. Lomov S.V, Akkerman R., Verpoest I.**, *Carbon composites based on multiaxial multiply stitched preforms. Part 5: Geometry of sheared biaxial fabrics.* Composites part A, *37(2006): 103-113*

10 **ASTM Standard** D 3518/D 3518M–94 (Reapproved 2001), "Standard Test Method for In-Plane Shear Response of Polymer Matrix Composite Materials by Tensile Test of a ±45° Laminate", 1994

11 **Chamis C.C.** Mechanics of composite materials: Past, present and future. *J Compos Technol and Research*, 11(1): 3-14 (1989).

12 **Lomov S.V., Ivanov D.S., Verpoest I., Zako M., Kurashiki T., Nakai H., Hirosawa S.** Meso-FE modelling of textile composites: Road map, data flow and algorithms**,** *Compos Sci Technol*, 67(9): 1870-1891 (2007).

13 **Cordebois, J.P., Sidoroff F.**, Damage induced elastic anisotropy, In: Mechanical behaviour of anisotropic solids. 1982, Martinus-Nijhoff. 761

14 Failure criteria in fibre reinforced polymer composites: **The World-Wide Failure Exercise**, ed. M.J. Hinton. 2004: Elsevier Science Ltd.

15 **Skudra A.M.,** Micromechanics of failure and reinforced plastics, In: Failure Mechanics of Composites, series Handbook of Composites, Elsevier Science Publishers B.V., 1986.